Improved Lateral Trajectory Prediction through En Route Air-Ground Data Exchange

David R. Schleicher[†], Ed Jones[º], Darren Dow[*]

Seagull Technology, Inc., Campbell, CA 95008

Richard A. Coppenbarger[‡]

NASA Ames Research Center, Moffett Field, CA 94035

Abstract

In generating advisories, current ground Air Traffic Management (ATM) automation tools such as NASA's Center-TRACON Automation System (CTAS) and MITRE's User Request Evaluation Tool (URET) rely upon an aging ground ATM infrastructure to provide current state and to predict future intentions of aircraft. Significant improvement in these advisories could be achieved by tapping into the high-precision state and intent data available onboard today's air transport aircraft. A recent NASA/FAA data exchange experiment was conducted to assist in quantifying the potential of datalink to improve ground-based ATM automation performance. This paper reports the results of a study into the quantitative characteristics of the improved lateral intent information and its potential impact on automation conflict detection performance. The results suggest that the downlink of flight management system (FMS) state and intent data will significantly improve the performance of current technology ground automation.

[†] Senior Systems Engineer, Air Transportation Group;
E-mail: dschleicher@seagull.com. Senior Member, AIAA.

[º] Manager, Commercial Products Group;
E-mail: ejones@seagull.com.

[*] Software Engineer, Software Engineering Group;
E-mail: ddow@seagull.com.

[‡] Aerospace Researcher, Automation Concepts Research Branch;
Mail Stop 210-10; E-mail: rcoppenbarger@mail.arc.nasa.gov.
Member, AIAA.

Introduction

Joint NASA/FAA research to evaluate the potential impact of a live air-ground data exchange has recently been concluded . This joint research, known as the En Route Data Exchange (EDX) Project, investigated the feasibility and operational benefits of sharing information between users and the ATM system. This most recent Phase 2 part of the EDX Project involved the real-time downlink from Honeywell Flight Management Systems (FMS) onboard revenue-carrying United Airlines (UAL) B777 aircraft to a CTAS research lab at NASA Ames Research Center (see Figure 1).

A recent series of analyses were conducted into the potential lateral trajectory prediction enhancements afforded by the data downlink of FMS-provided state and intent data. These analyses included:

1) **Input Comparison Analysis**: comparing the FMS downlinked information to information obtained from current surveillance, modeling, and flight planning sources;

2) **Trajectory Prediction Analysis:** comparing trajectories synthesized from FMS downlinked information versus current CTAS predictions;

3) **Lateral Route Intent Analysis:** comparing FMS intent as inferred from the downlinked Active and Active+1 waypoints versus the Host flight plan (with amendments); and

4) **Conflict Detection Analysis:** comparing anticipated performance of conflict detection and resolution decision support tools with and without FMS downlink.

The results of the first two analyses were previously reported in Ref. 1. The details of the final two are summarized herein. For more details on these EDX Phase 2 analysis results, see Ref. 2.

The EDX Phase 2 field evaluation involved downlinking aircraft state, performance, preference, and intent data from United Airline's Boeing 777 FMS-ACARS-equipped operational airline flights through Denver ARTCC (ZDV) airspace. The downlink was accomplished over the existing VHF ARINC ACARS Data Network System (ADNS). The aircraft downlinked data are received from the ACARS Ground Station via modem to the EDX laboratory at NASA Ames Research Center, where they are retained in data files.

Forty-eight B777 aircraft were equipped with EDX downlink capability over the course of the EDX Project. The equipped EDX aircraft downlinked a set of primary parameters at a nominal rate of once per minute, along with a number of secondary parameters that may be useful in future analyses (see Ref. 1). The primary parameters included FMS-derived aircraft position, velocity, and Active and Active+1 waypoint intent data.

Data Analysis Process

The overall data analysis process is illustrated in Figure 1. The EDX data is made available to the Lateral Route Intent Analysis, along with the other nominal trajectory prediction input data (Host track and flight plan data and Rapid Update Cycle (RUC 2) atmospheric data) that are normally used by CTAS. To support the Trajectory Prediction Analysis, the input data are fed to a Baseline version and a specially modified EDX version of CTAS. Details of the EDX CTAS modifications are presented in Ref. 3, but basically the modifications allow CTAS to utilize EDX data in lieu of its nominal sources. The Trajectory Prediction Analysis analyzes the comparative outputs of the respective versions of the CTAS Trajectory Synthesizer (TS) module (see Ref. 4) to determine improvements relative to the observed truth trajectories. Finally, the outputs of the Lateral Route Intent Analysis and Trajectory Prediction Analysis provide the input data required for the Conflict Detection Analysis.

Lateral Route Intent Analysis

The Lateral Route Intent Analysis compares the differences in the planned horizontal route constructed with and without the incorporation of EDX waypoint information from the aircraft FMS. It should be noted that route intent is intrinsically dynamic in nature – Host route intent is affected by flight path amendments entered by the controller, while EDX route intent was affected by pilot inputs into the FMS.
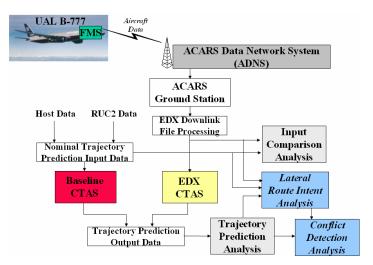

Figure 1 EDX Phase 2 Data Analysis Process

Accordingly, the Host lateral intent at a given time was taken to be the original Host flight plan adjusted by any flight plan update messages received from the Host computer up to that point. The FMS lateral intent was inferred by adjusting the current instantaneous Host flight plan with the FMS Active and Active+1 waypoints as most recently received from the EDX data. Downstream of the FMS Active and Active+1 waypoints, it was assumed that the FMS flight plan rejoined with the instantaneous Host flight plan.

A major issue was discovered in the lateral intent analysis having to do with the design of the downlink process. In the original EDX Phase 2 experiment planning, it was decided to use only four characters to represent waypoints. In real-world operations, a large number of flights utilized 5-character waypoints, resulting in waypoint name ambiguities in the collected database. Fortunately, range and bearing to next waypoint were also downlinked, so we were able to resolve many of the ambiguities, especially in post-processing mode (real-time mode would only be able to resolve the next waypoint using range/bearing, and downstream predictions would still have problems). Naturally, we recommend that future implementations of FMS intent downlink use a 5-character representation for the waypoint name and continue to downlink next-waypoint range/bearing to further enhance data integrity.

Lateral Trajectory Prediction Model

To help automate the Lateral Route Intent Analysis, a simple trajectory prediction model was developed. This trajectory prediction model constructed the Host lateral intent and FMS lateral intent at a given point in the trajectory, and predicted the aircraft's path

American Institute of Aeronautics and Astronautics

along each respective intended plan for a prescribed fly-out time into the future. The respective lateral intent errors were then computed at each prediction point as the distance difference between the predicted intent point and the corresponding point on a path recorded from Host radar truth. Even though the downlinked GPS/INS position measurement is intrinsically more accurate, we used Host radar truth as a common basis to be consistent with the Baseline CTAS and EDX CTAS, which reset the prediction at each major cycle to the current radar position. The intent errors were resolved into cross-track and along-track components, relative to the radar truth path. We then advanced the start point a prescribed time step (nominally 12 seconds to coincide with the normal Host update cycle), reset the current location to coincide with Host radar truth, and predicted the respective lateral paths and corresponding errors for the next prediction "window." This process was repeated until one of the data sources had been exhausted for that flight.

This prediction technique closely mimics the way that the CTAS Trajectory Synthesis (TS) model works, as illustrated in Figure 2, which compares the simple lateral prediction algorithm with the CTAS trajectory synthesizer operating on the same March 11th Denver arrival flight. Referring to the figure, the upper half shows the performance of the simplified trajectory prediction model as it projects along the Host flight plan and FMS intent as inferred from the downlinked Active and Active+1 waypoints. In this case, as was typical, the FMS intent followed the truth trajectory (as measured by the Host radars) quite accurately (indistinguishable at the scale of the figure).

Readily evident in the figure, the simplified prediction model attempts to accurately portray the waypoint switching logic employed by the CTAS Trajectory Synthesizer to correct itself when the Host flight plan is not being followed, as detected by the radars. The trajectory predictions are made repeatedly every time step, starting from the current location as measured by the radars. The switching logic applies rules to infer whether the current "next waypoint" truly represents intent, or whether the intended next waypoint should be switched to a downstream waypoint. As illustrated in the figure, the simplified logic does a credible job of emulating the CTAS waypoint-switching behavior. The one major difference is that the CTAS version infers that the final waypoint switch is to a waypoint further downstream, the metering fix. Also notable is the curvature of the CTAS-predicted trajectories in

comparison to the simplified model, which assumes straight-line flight between waypoints.

The successful emulation of the CTAS Trajectory Synthesizer is significant. It enabled us to examine a much greater number of flights than would have been practical using CTAS. The reason for this is that we could automatically execute the simplified model in a batch "script" that can operate on a large data set in "fast-time". Further, we were able to incorporate features into the analysis script that accommodates anomalies in the data, most notably, an accommodation of FMS waypoint ambiguities as discussed previously.
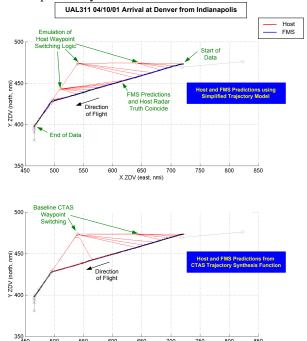

Figure 2 Typical Arrival Showing a Comparison of Trajectory Prediction Methods

Figures of Merit (FOMs)

The primary figures of merit (FOMs) for the Lateral Route Intent Analysis are the Host Lateral Route Intent Error (HLRIE) and FMS Lateral Route Intent Error (FLRIE). The HLRIE is defined as the difference between the radar truth trajectory and the Host flight plan (with updates) as extrapolated over a "projection window" (nominally 20 minutes to coincide with the planning horizons of typical decision support tools). Similarly, the FLRIE is defined as the difference between the radar truth trajectory and the inferred FMS intent as extrapolated over the projection window.

To calculate the differences between planned and actual trajectories over the projection window, we computed difference samples at a one-second interval and computed the mean and standard deviation of these samples over the projection window. The LNAV flag available in the FMS downlink is an indication of whether the FMS is engaged or the aircraft is being vectored. Accordingly, we ignored all windows when the LNAV flag indicated that the FMS was disengaged.

In addition to the magnitude of the HLRIE and FLRIE, the figures of merit were also resolved into cross-track and along-track components, relative to the radar truth path. The moving window average of all these FOMs was then calculated over each flight. In addition, we recorded which projection window exhibited the maximum HLRIE and FLRIE, and what that maximum value was. We also recorded which projection window contained the largest average HLRIE and FLRIE, and recorded that value as well.

We then grouped the flights into separate data sets for Arrivals, Departures, and Overflights and calculated ensemble means and ensemble standard deviations of all flights in the respective data set. In all, 191 Arrivals, 166 Departures, and 204 Overflights (561 flights in total) were analyzed in this way; the flights occurred from February through early April of 2001. Finally, we calculated "histograms" that show the distribution of how many flights in each category (Arrivals, Departures, Overflights) exhibited HLRIE and FLRIE FOMs in size "bins" ranging from less than 2 nautical miles (nmi) to over 50 nmi. Histogram analysis is explained more thoroughly in the next section.

Key Results
Downlinked FMS intent significantly reduces the average and maximum lateral intent error for Arrivals, Departures and Overflight. Figure 3 summarizes the average and maximum HLRIE and

FLRIE for the flights examined in the study. For Arrivals, the reduction in the average lateral route intent error is considerable – a reduction from over 6 nmi to 1.72 nmi. The ensemble standard deviation, which indicates the "dispersion" of the data about the mean, is also tightened up remarkably from 5.51 nmi down to 1.89 nmi. The averages are reduced considerably in the Departures and Overflights categories as well, although not quite as dramatically as the case with Arrivals. The improvements in the maximum columns are deceivingly conservative. Most of the maximum conditions for the downlinked FMS cases were very short-lived – they occurred primarily during times when FMS Active and Active+1 transitions were occurring. We believe that a more careful implementation of the FMS intent downlinking process would eliminate these transient effects.

A significant population of flights exhibit a mean Host Lateral Intent Error (HLRIE) greater than 4 nmi, the nominal US IFR airway half-width. While these ensemble statistics are interesting and representative of the overall improvement achievable by FMS intent downlink, it is even more revealing to look closely at the distribution of the number of flights with HLRIE levels in certain ranges. Figure 4 presents a histogram summary plot of the results. As shown, over 54% of the Arrivals exhibited mean HLRIE values greater than 4 nmi. Correspondingly, 25% of the Departures and only 4% of the Overflights showed a mean HLRIE greater than 4 nmi. Notable in the histogram plot is the large population of Arrivals with HLRIE values in the 12 to 18 nmi bins. We believe this stems from a practice where the aircraft gets cleared to a downstream waypoint (probably the metering fix) – the FMS Active waypoint is updated in accordance with this clearance, but the Host flight plan is not updated for one reason or another.

Figure 3 Average and Maximum Lateral Route Intent Error for 561 Flights

	191 Arrivals				166 Departures				204 Overflights			
	Average		Maximum		Average		Maximum		Average		Maximum	
	HLRIE	FLRIE	HLRIE	FLRIE	HLRIE	FLRIE	HLRIE	FLRIE	HLRIE	FLRIE	HLRIE	FLRIE
Ensemble Mean (nmi)	6.06	1.72	16.24	11.09	2.46	1.53	7.79	6.06	1.09	0.47	4.35	2.78
Ensemble Std Dev (nmi)	5.51	1.89	11.44	9.96	2.32	1.89	8.65	6.24	1.48	0.59	6.01	5.04

Mean Host Flight Plan Deviations from Radar Truth
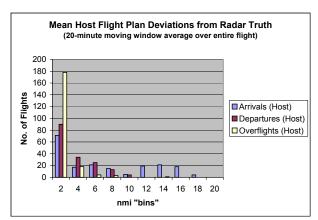(20-minute moving window average over entire flight)

Figure 4 Histogram Plot of No. of Flights with Certain HLRIE Levels

Downlinked FMS Intent greatly reduces the population of flights exhibiting mean Lateral Intent Errors greater than 4 nmi (see Figure 5). As shown, the number of Arrivals exhibiting mean FLRIE values greater than 4 nmi is reduced to 13% of the 191 population (compared to 54% for the HLRIE). For Departures, the mean FLRIE was reduced also to 13% of the 166 population (as compared to 25% HLRIE) and none of the Overflights showed a mean FLRIE over 4 nmi (as compared to 4% HLRIE). Also notable in Figure 5 is that the previous population of Arrivals with HLRIE's in the 12-18 nmi bins is eliminated.
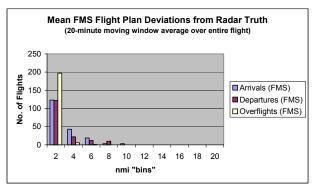
Mean FMS Flight Plan Deviations from Radar Truth
(20-minute moving window average over entire flight)

Figure 5 Histogram Plot of No. of Flights with Certain FLRIE Levels

The preceding analyses focused on a representative 20-minute projection window. An interesting point of investigation is to determine to what degree the FMS intent downlink (Active and Active+1 waypoints) supports a 20-minute planning window. Accordingly, for each 12-second time step through the data, we determined the amount of flight time represented by the Active and Active+1 waypoints from the current position and velocity. We then calculated the mean "look-ahead" time represented by the two FMS waypoints over the flight. For Arrivals, the average look-ahead time represented by downlinked FMS Active and Active+1 waypoints was 13.2 minutes; for Departures and Overflights the corresponding average look-ahead times were 33.5 and 37.5 minutes, respectively. The distribution of average look-ahead times among Arrivals, Departures and Overflights is presented in Figure 6.
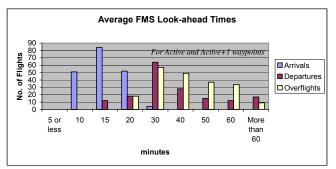
Average FMS Look-ahead Times

Figure 6 Histogram of Average Look-ahead Times Afforded by Two FMS Waypoints

Conflict Detection Analysis

The use of EDX downlinked data by future ATM automation conflict probes will improve the accuracy of conflict detection methods. Current technology conflict probes have to contend with the inherent inaccuracies of radar-based position and velocity measurement and the limitations of Host flight plan data when controllers do not keep the Host computer intent model up to date. Downlinked data from an aircraft's FMS should offer considerable increases in current position, current velocity, and intent accuracy.

Existing State and Intent Data Accuracies

In flight, FMS-equipped jet aircraft position and ground speed errors will typically be based on sophisticated inertial and GPS avionics. On the ground, the accuracy of ATC sensing of aircraft position and speed will be limited to ground radar sensing and data processing systems. Typical GPS-derived and Radar-derived one-sigma surveillance errors are shown in Figure 7.

American Institute of Aeronautics and Astronautics

	GPS-derived	Radar-derived
Position error, σ_p (nmi)	0.0055[1]	0.45[2]
Ground Speed error, σ_v (nmi/min)	0.0042[3]	0.26[4]

[1]based on 10.2 m Selective Availability (SA)-off, GPS horizontal position error from Ref. 5

[2]assuming measurement uncertainty based on mosaiced Air Route Surveillance Radar (ARSR) radar from 100 x 100 nmi range from Ref. 6

[3]based on 0.13 m/s Selective Availability (SA)-off, GPS ground speed error performance from BAE Systems ALLSTAR GPS receiver from Ref. 7

[4]based on 15.5 kt standard deviation Overflight ground speed error from Ref. 1.

Figure 7 Typical FMS and Host-derived Current Position and Velocity Errors

Specific current position and velocity errors will be a function of a multitude of factors including (for GPS-derived data): the relative positions of a GPS receiver and the satellites it is tracking; and (for radar-derived data): range and azimuth from radars, single-sensor vs. mosaicing, radar registration, non-Mode C altitude estimation, antenna tilt and skew, refraction, coordinate conversion and timing uncertainties. In general, these errors will range significantly based on scenario-specific factors. For example, radar-derived position error will typically vary between 0.15 nmi to 0.9 nmi based purely on range from the radar source (see Ref. 7). However, as one surmises from Figure 7, the typical radar-derived data current position and velocity errors are on the two orders of magnitude greater than that derived by using GPS data.

In addition to the improved state information, better predictions on lateral intent due to downlinked FMS-based intent data should improve conflict probe prediction accuracy. Previous investigations have shown the percentage of route clearances reflected in Host flight plan amendments to be as low as 18% (see Ref. 8). Using the EDX and Host flight plan intent data collected during the Phase 2 field test, one may derive an intent-based predicted position error, σ_i, as a function of lookahead time. The method used for determining σ_i is as follows. For a given aircraft flight and lookahead time, the Simple Trajectory Prediction Model (explained in the previous section) was used to project an aircraft forward in time, a given τ minutes ahead, along its flight plan. (Note: the varying ground speed in our predictions matched the actual sensed ground speeds, and, therefore, uncouples the prediction error based purely on horizontal intent from that based on the ground speed.). Then, at time τ, the aircraft's actual position (based on Host radar data) was compared with the aircraft's predicted position and the relative position (with distance, D, and lateral and longitudinal components, x and y, respectively), were determined (see Figure 8). (Note: because of the ground speed matching, lateral deviations over time result in both cross-track and along-track position errors.)
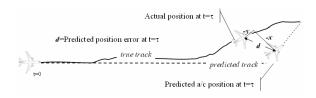

Figure 8 Intent-based Predicted Position Error Determination

This data was collected for:
- all valid lookahead time windows from 5 to 30 minutes,
- all Arrival, Departure, and Overflights,
- EDX and Host flight plan-based intent data, and
- only cases where the LNAV flag was "on" (Note: future conflict probes that receive LNAV "off" information are presumed to revert to a velocity-vector-based trajectory prediction).

Next, a representative prediction error deviation due to intent, σ_i, was determined for both EDX and Host data cases for lookahead times ranging from 5 to 30 minutes. For a given lookahead time and data case, σ_i was calculated by first determining the two-dimensional mean and standard deviation values: $\bar{x}$, $\bar{y}$, σ_x, and σ_y, respectively. Then, we assumed $\bar{x}, \bar{y} = 0$ over large numbers of aircraft trials because of no known biasing phenomena (and, in the case of a consistent bias error, a good conflict probe would seek to improve its predictive model to take out such a bias). Finally, we calculated a representative σ_i assuming that the predicted position variances were composed of non-correlated x and y-based position variances, such that $\sigma_i^2 = \sigma_x^2 + \sigma_y^2$ (for a citation of a similar calculation for a horizontal 2D standard deviation quality measures for GPS position accuracy, see Ref. 9). The determined σ_i for Arrivals, Departures, Overflights, and all aircraft, for both EDX and Host data cases, are shown in Figure 9.
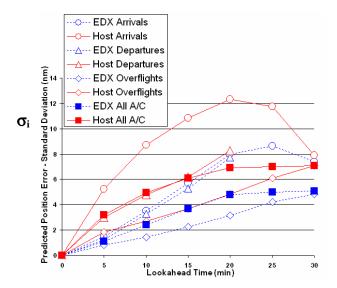
Figure 9 EDX and Host Intent-based Predicted Position Error as a Function of Lookahead Time

Figure 9 illustrates that arrivals exhibit a maximum intent-based predicted position error at 20 minute lookahead times, while overflights exhibit increasing errors beyond 30 minute lookahead times. The primary reason for this is the natural convergence of potential arrival routes at larger lookahead times.

As we expected, the downlinked EDX waypoint information provides significant reductions in predicted position error over that found in predictions based on Host flight plans. However the potential reduction in predicted position error due to use of EDX data is a function of both lookahead time and phase of flight.

The greatest reductions in intent-based predicted position error occur for the arrival phase of flight for moderate lookahead times of 10 to 20 minutes. The arrival phase of flight was expected to provide the most fruitful opportunity for EDX improvement because of the previously noted greatest Host Lateral Intent errors (see Figure 4). The moderate lookahead times for Arrivals offer the greatest potential benefit (i.e., greatest $\sigma_i\big|_{Host} - \sigma_i\big|_{EDX}$) because they are the lookahead times where the Active and Active+1 waypoints are valid. Beyond Active+1 waypoints, the EDX predicted intent reverts back towards that of the Host predicted intent. Overall, the Arrival σ_i increases up to 20 minutes lookahead and then decreases. This occurs because of the convergence of potential Arrival routes for larger lookahead times.

Departures exhibit values of σ_i less than Arrivals, but greater than Overflights and an overall potential

reduction in predicted position error that peaks at 5 minutes lookahead. Note: that values of σ_i for lookahead times of 25 and 30 minutes were deemed statistically insignificant.

Overflights exhibit a steadily increasing σ_i, but a slowly growing potential reduction in predicted position error that are greatest at the furthest lookahead time. This is primarily because of the large typical lookahead times for Overflight Active and Active+1 waypoints (see Figure 6).

When averaging σ_i over all valid flights, we obtain significant reductions in σ_i throughout the "All" lookahead times.

Having convinced ourselves that downlinked EDX position, ground speed, and intent data are likely to improve our conflict probe performance, the key question is *By how much?*

Conflict Detection Performance Analysis Methodology and Results

A number of previous analytical and real-time conflict probe-based analyses of stochastic conflict detection performance have been performed Refs. 10-14. In this effort, an alternative method to determine order of magnitude impacts on conflict probe performance was developed and implemented and is now explained.

For the purposes of simplicity, a two-dimensional conflict test case was posed. This test case consisted of two jet aircraft with a 90 deg crossing conflict at an arbitrary initial range and bearing from each other. Both aircraft are flying level in en route airspace at a constant ground speed of 450 kts with no wind. A conflict probe is predicting the aircraft conflict using a flight-plan-based intent model for each aircraft. The flight plan-based predicted track error exhibits the statistical behavior previously analyzed. No traffic flow management constraints are active. The initial conditions are shown in Figure 10.
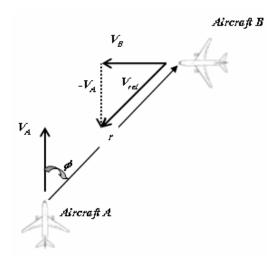
Figure 10 Conflict Detection Test Case: Aircraft A-Relative Reference Frame Geometry

Now, we will assume that the predicted position error for a given aircraft at a future time, τ, can be represented by the expression, $\sigma_{p,p}$. Assuming that this predicted position error can be decomposed into independent, Gaussian, random, predicted position errors due to current position, current velocity, and intent, σ_p, σ_v, and σ_i respectively, we can derive the expression:

$$\sigma_{p,p}^{\ 2}(\tau) = \sigma_p^{\ 2} + \tau^2 \sigma_v^{\ 2} + \sigma_i^{\ 2} \qquad (1)$$

Taking the values for GPS and radar-derived σ_p, σ_v and σ_i previously derived from Figures 7 and 9 for values of lookahead time between 0 and 30 minutes, we can calculate $\sigma_{p,p}^{\ 2}$ and its individual components. The individual variances of the 3 components for both EDX and Host data in both Arrival and Overflight cases were calculated and are shown in Figures 11 and 12.
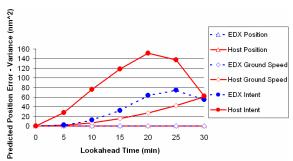

Figure 11 EDX and Host-derived Predicted Position Component Variances: Arrivals
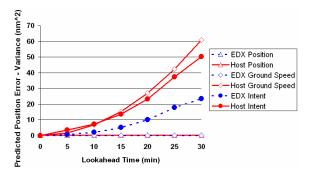

Figure 12 EDX and Host-derived Predicted Position Component Variances: Overflights

The results of Figures 11 and 12 show that, for Arrivals, significant intent errors dominate the variance of predicted future positions up to 30 minute lookahead times. Velocity errors dominate the variance of predicted future positions for both longer lookahead times for Arrivals and generally for all non-Arrivals. EDX intent and velocity data offer significant reductions in predicted position variance from baseline Host-data levels, except in the case of long lookahead time Arrivals (> 25 min). In both EDX and Host data cases, current position errors are negligible, and, in the EDX case, the current velocity error is negligible as well.

Next, Equation (2), derived in Ref. 14, describes the variation in aircraft conflict miss distance as a function of the predicted trajectory position accuracy at the point of closest approach for Aircraft A and B:

$$\sigma_{r_f} = \sqrt{\sigma_{p,p,A}^{\ 2} + \sigma_{p,p,B}^{\ 2}} \qquad (2)$$

Assuming that the predicted position error for each aircraft will be the same, we ultimately derive:

$$\sigma_{r_f} = \sigma_{p,p}\sqrt{2} \qquad (3)$$

In previous Seagull conflict probe analysis research (see Ref. 11), the probability of conflict for a 2D, two aircraft conflict was analytically derived as:

$$P(conflict) = \frac{1}{2} erf(\frac{R + r_f}{\sqrt{2}\sigma_{r_f}}) + \frac{1}{2} erf(\frac{R - r_f}{\sqrt{2}\sigma_{r_f}}) \qquad (4)$$

where:

R is the Protected Airspace Zone radius,

r_f is the separation at the closest point of approach (CPA), and

σ_{r_f} is the one sigma minimum separation error.

Equation (4) can, in turn, be used to determine the probability of conflict for our test case for arbitrary initial relative distance and bearing (of Aircraft B from Aircraft A). These conflict probabilities can

American Institute of Aeronautics and Astronautics

then be plotted in the relative Aircraft A reference frame, thus creating a "conflict probability map" (similar to what has been done previously in Ref. 14).

For the theoretical case of perfect current and future knowledge of aircraft states (i.e., $\sigma_p = \sigma_v = \sigma_i = 0$), the conflict probability map would look like Figure 13. In this case, any intruder aircraft initial conditions within Region I would yield P(conflict)=1.0 (i.e., 100% probability of correctly identifying the conflict) and those within Region II would yield P(conflict)=0.0. In this special case, the P(false alarm)=P(missed alerts)=0 and P(correct alerts)=1.0. Note: we assume that "correct alerts" consist of both an *alert* if the intruder aircraft eventually violates the Protected Airspace Zone (PAZ) or *no alert* if there is no such eventual violation.
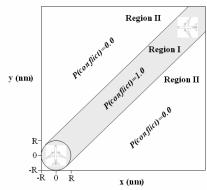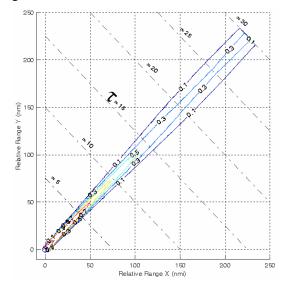

Figure 13 Conflict Prediction Probability Map assuming Perfect Knowledge
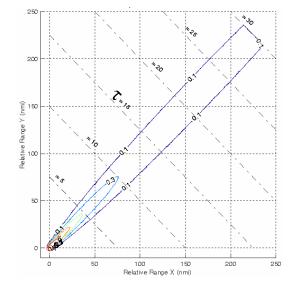
In the practical case of imperfect current and future knowledge of aircraft states (i.e., $\sigma_p, \sigma_v, \sigma_i > 0$), the conflict probability map will look similar to those in Figure 14. In this case, any aircraft initial conditions will yield P(conflict)<1.0 and the probability map will yield a contour plot of conflict probabilities with P(conflict) getting smaller with distance from the Protected Airspace Zone. In the imperfect case, P(false alarm), P(missed alerts), and P(correct alerts) are between 1.0 and 0.0. Then, depending on the given initial conditions, either P(correct alerts) + P(missed alerts) = 0 (in the case of an intruder aircraft's initial conditions in Region I of Figure 13) or P(correct alerts) + P(false alarms) = 0 (in the case of an intruder aircraft's initial conditions in Region II of Figure 13).

Going back to our conflict detection test case to quantify the expected impacts of EDX downlinked data on conflict detection performance, we first assume a value of 5 nm for R, the diameter of the PAZ, which equals the nominal en route US airspace

separation standard. Then, we calculate σ_{r_f} from Equation (3) and the data in Figure 9. Finally, we determine r_f based on conflict geometry, and we use Equation (4) to derive a conflict probability map for a given set of r, ϕ initial conditions and for either EDX or Host Data cases. Conflict probability maps for EDX and Host data cases were developed for the Arrival and Overflight data. The Arrival results are shown in Figure 14. In order to better understand the relative impact of EDX data, the two conflict probability maps were differenced and are shown in Figure 15.

a) EDX Data

b) Host Data

Figure 14 Conflict Probability Maps for EDX and Host-based data: Arrivals
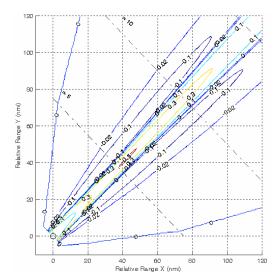
Figure 15 Differenced EDX-Radar Conflict Probability Map: Arrivals

The conflict probability maps in Figure 14 display what we expected: isoprobability lines that extend further out in time and wrap more tightly around the PAZ for predictions using the higher precision EDX data. The differenced conflict probability maps in Figure 15 show the general trend of positive probability differences along the conflict centerline and pockets of negative probability differences just outside the extended 45 degree lines from the edges of the PAZ. These differences can be interpreted as quantitative EDX-based reductions in conflict probe missed alert and false alarm rates as follows.

Taking the conflicting case first (i.e., the intruder is in Region I of Figure 13), let's assume the predicted probability of conflict using Host data is *P(Host)* for a given initial relative position. Since, based on the initial position, we know that the aircraft will be in conflict, P(correct alert)=*P(Host)*. This also means that P(missed alert)=1-*P(Host)*. Now, looking at Figure 15, we notice that the differenced (EDX-Host) probabilities for a given initial position are some value, δ, such that the predicted probability of conflict using EDX data is δ greater than the predicted probability of conflict using Host data. This means that *P(EDX)=P(Host)+δ*. Therefore, P(correct alert) using the EDX data is greater than P(correct alert) using the Host data by δ, and, likewise, the P(missed alert) using the EDX data is less than P(missed alert) using the Host data by δ.

A similar analysis can be done for the non-conflicting case to show that P(false alarm) using the EDX data is less than the P(false alarm) using the Host data by -δ. Thus, the difference statistics in Figure 15 provides a map for expected missed alert and false

alarm impacts of EDX downlink data for all relative aircraft initial conditions. Close inspection of Figure 15 reveal the order-of-magnitude missed alert and false alarm impact statistics for our crossing conflict probe test case and are shown in Figure 16.

Missed Alert Rate Impact	False Alarm Rate Impact
At 6 minutes lookahead time for a crossing collision, missed alert rates drop a maximum of 50%. Longer lookahead times result in smaller missed alert rate reductions approaching 10%.	For lookahead times between 0 and 13 minutes for "near-conflicts" with minimum separation distances roughly 2*PAZ diameter, false alarm rates drop a maximum of 10+%.

Figure 16 Order of Magnitude EDX Missed Alert and False Alarm Rate Impacts for Arrivals

For the analysis conducted, missed alert rate reductions can be as high as 50% in the case of arrivals and can provide 30+% reductions for overflights. False alarm rate reductions are lower than the missed alert rate reductions, and are expected to decrease 10+% or less. Specific reductions in missed detection and false alarm rates will vary based conflict initial conditions, the specific position, velocity, and intent errors experienced, and other factors not accounted for (such as wind prediction errors).

Conclusions

In the work reported on in this paper, a number of key findings can be identified. First of all, downlinked FMS intent significantly reduces the average and maximum lateral intent error. The reduction in the average lateral route intent error is greatest for Arrivals, but considerable for Departures and Overflights as well.

The future value of downlinking only Active and Active+1 waypoints will be limiting in the case of a current technology conflict probe lookahead time (~20 min) for Arrival aircraft. Designers of next generation surveillance systems such as Automatic Dependent Surveillance-Broadcast (ADS-B) should consider broadcasting additional waypoints.

In terms of contributing to overall predicted position variance, the overwhelmingly important components are intent and current velocity. For Arrivals, significant intent errors dominate the variance of predicted future positions up to 20 minute lookahead times. Velocity errors dominate the variance of predicted future positions for both longer lookahead times for Arrivals and generally for all non-Arrivals.

Downlinked FMS data are expected to significantly reduce missed detection and false alarm and alert rates of current technology conflict probes. Potential

missed alert rate reductions of as high as 50% for arrivals were calculated; expected false alarm rate reductions are lower than the missed alert rate reductions, on the order of 10% or less. Specific reductions in missed detection and false alarm rates will vary based conflict initial conditions, the specific position, velocity, and intent errors experienced, and other factors not accounted for (such as wind prediction errors).

The results presented here suggest that significant benefits could be obtained in trajectory predictions and subsequent ATC advisories arising from specific ATM automation incorporation of live, downlinked EDX data. Some of the ATM decision support tools that could benefit include CTAS' Direct-To, Conflict Probe, Traffic Management Advisor, and En Route Descent Advisor automation and MITRE's URET. Future work should aim at validating the potential benefits through comparison of the performance of these specific ATM automation tools with and without the data exchange.

The beneficial impacts of the downlinked EDX data performed in this effort are just the dawn of a new era in planned ATM service improvements leveraging the addressed data link. Recently released Ref. 15 details many new one-way and two-way data link-enabled ATM services envisioned for all flight domains. Future analyses similar to this one will need to be performed to predict and validate the potential impacts of the new data link-enabled ATM services.

Acknowledgement

References

[1] Coppenbarger, R. A.; Kanning, G.; and Salcido, R.; "Real-Time Data Link of Aircraft Parameters to the Center-TRACON Automation System (CTAS)," 4th USA/Europe ATM R&D Seminar, Sante Fe, NM, Dec. 3-7, 2001.

[2] Jones, E., and Schleicher, David R., "NASA/FAA En Route Data Exchange (EDX) Phase 2 Field Evaluation Final Report (Period Jan. 2001 – Dec. 2001), TM 00216-01, Seagull Technology, Inc., December 2001.

[3] Coppenbarger, R., Weidner, T., Schleicher, D., "En Route Data Exchange Phase 2 (EDX-2) Field Evaluation, CTAS Software Requirements, Version 2.0," February 2000.

[4] Slattery, R. A., Zhao, Y., "En route Descent Trajectory Synthesis for Air Traffic Control Automation," *Proceedings of the American Control Conference*, Seattle, WA, June 1995.

[5] Parkinson, B., and Spilker, J., *Global Positioning System: Theory and Applications: Volume I*, Progress in Astronautics and Aeronautics-Volume 163, AIAA, Washington, DC, 1996.

[6] McVeigh, M., and Drew, D., "Accuracy of Position Data Using Mosaic Techniques," *Journal of ATC*, January-March 2001, pp. 7-18.

[7] BAE Systems, Specification Sheet for ALLSTAR GPS Receiver, ALLSTAR DGPS-1, August, 1999.

[8] Lindsey, K., "Currency of Flight Intent Information and Impact on Trajectory Accuracy," FAA/Eurocontrol Technical Interchange Meeting on Shared Flight Intent Information and Aircraft Intent Data, October 25, 2000.

[9] Quality Engineering and Survey Technology Ltd., "Accuracy Measures," "http://www.mercat.com/QUEST/Accuracy.htm 1998.

[10] Krozel, J., Peters, M., and Hunter, G., "Conflict Detection and Resolution for Future Air Transportation Management," TR97138-01, Contract NAS2-14285, Seagull Technology, Inc., Los Gatos, CA, April 1997.

[11] Brudnicki, D. J., and McFarland, A. L., "User Request Evaluation Tool (URET) Conflict Probe Performance and Benefits Assessment," MITRE Center for Advanced Aviation System Development, CAASD Rept. MP98W0000112, McLean, VA, June 1997.

[12] Cale, M.L., Paglione, M., Ryan, H., Timoteo, D., and Oaks, R., "User Request Evaluation Tool (URET) Conflict Prediction Accuracy Report," Dept. of Transportation/Federal Aviation Administration, Rept. DOT/FAA/CT-TN98/8, April 1998.

[13] Weidner, T., Davidson, T.G., and Dorsky, S., "En Route Descent Advisor (EDA) and En Route Data Exchange (EDX) ATM Interruption Benefits," TR00188.26-01f, NASA Contract NAS2-98005, Seagull Technology, Inc., Los Gatos, California, December 2000.

[14] Bilimoria, K. D., "Methodology for the Performance Evaluation of a Conflict Probe," AIAA Journal of Guidance, Control, and Dynamics," Vol. 24, No. 3, May-June 2001, pp. 444-451.

[15] RTCA SC-194, "Concepts for Services Integrating Flight Operations and Air Traffic Management Using Addressed Data Link," RTCA DO-269, RTCA, Inc., Washington, DC, June 12, 2001.

Biographies

David R. Schleicher

Dave Schleicher graduated from Princeton University with a Bachelor's degree in Mechanical and Aerospace Engineering summa cum laude in 1988. After acquiring his Master's degree in Aeronautics and Astronautics from Stanford University in 1990, Dave Schleicher joined NASA Ames Research Center and worked on advanced aircraft systems analysis. While at NASA-Ames, Dave transitioned to air traffic management research as one of the initial developers of NASA's Advanced Air Transportation Technology (AATT) research program. Since 1997, Dave has been working at Seagull Technology, where he has been performing ATM systems engineering to support new air traffic management operations concepts, decision support tool technology, and analytical and simulation evaluations of their performance. His recent research activities have focused on small airport and en route ATM decision support systems, and air-ground datalink experiments. Dave is a Senior Member of AIAA and also holds a private pilot's license.

Ed Jones

Ed Jones holds an M. S. degree in Aeronautics and Astronautics form M. I. T. Since joining Seagull Technology in 1996 as a Program Manager, Mr. Jones has led a number of projects related to aircraft simulation and modeling, datalinks, navigation and control. He has led several projects involving ADS-B techniques for vehicle tracking and surveillance, augmented reality displays, aerial command and control systems, and data analysis. Mr. Jones is expert in data communications, computer networks and information systems.

Darren Dow

Darren Dow has a Bachelor's degree in Aerospace Engineering from San Jose State University. Mr. Dow has been employed at Seagull Technology for over 5 years. During this time, he has developed software for various decision support tool studies that involve the analysis of flight trajectories. He has also developed software for several applications that employ GPS, ADS-B and other aviation technologies and has experience in integrating hardware and software both in-house and in the field.

Richard A. Coppenbarger

Rich Coppenbarger, has been employed with NASA Ames Research Center at Moffett Field, California since 1989. During his tenure at Ames, Mr. Coppenbarger acquired a Masters degree in Aerospace Engineering from Stanford University. Mr. Coppenbarger has been involved with ATC automation research for the past three years. During this time, he has focused on data link research and en route decision-support-tool development under the AATT/CTAS project. His prior research activities at Ames included microburst wind shear accident investigation, and helicopter obstacle-avoidance guidance and control.